

ArticFlow: Generative Simulation of Articulated Mechanisms

Jiong Lin Jinchen Ruan Hod Lipson
 Creative Machines Lab, Columbia University
 New York, NY 10027

Abstract

Recent advances in generative models have produced strong results for static 3D shapes, whereas articulated 3D generation remains challenging due to action-dependent deformations and limited datasets. We introduce ArticFlow, a two-stage flow matching framework that learns a controllable velocity field from noise to target point sets under explicit action control. ArticFlow couples (i) a latent flow that transports noise to a shape-prior code and (ii) a point flow that transports points conditioned on the action and the shape prior, enabling a single model to represent diverse articulated categories and generalize across actions. On MuJoCo Menagerie, ArticFlow functions both as a generative model and as a neural simulator: it predicts action-conditioned kinematics from a compact prior and synthesizes novel morphologies via latent interpolation. Compared with object-specific simulators and an action-conditioned variant of static point-cloud generators, ArticFlow achieves higher kinematic accuracy and better shape quality. Results show that action-conditioned flow matching is a practical route to controllable and high-quality articulated mechanism generation.

1. Introduction

Generative models have become a leading approach for content generation across images, audio, and video. The model landscape has progressed from early variational autoencoders (VAEs) [19] and generative adversarial networks (GANs) [13] to flow based methods such as continuous normalizing flows (CNFs) [39, 44], diffusion models [14, 47], and, more recently, flow matching methods [23]. Building on this progress, recent work has increasingly turned to 3D content [9, 10], where geometric structures and physical constraints introduce additional challenges.

Broadly, two competing paradigms have emerged for 3D generation. The first leverages powerful 2D priors to synthesize multi-view consistent images and then lifts them to 3D; for example, Zero-1-to-3 [27, 46] style 3D synthesis pipelines. This family benefits from 2D foundation mod-

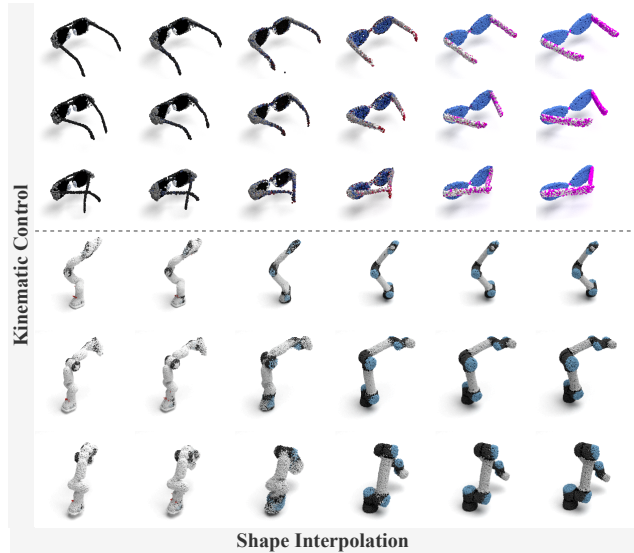


Figure 1. **ArticFlow** models a category of diverse articulated objects with a single point-flow field, conditioned on shape prior and joint actions. In this figure, columns interpolate the shape-prior condition (novel instances); rows sweep the action control (joint angles). Examples include eyeglasses from *PartNet-Mobility* [53] and robot arms from *MuJoCo Menagerie* [49]. The same field produces coherent deformations for one category of articulated shapes, enabling interpolation and controllable 3D generation.

els [45] pre-trained on high-quality image datasets, but often struggles with true 3D consistency and geometric fidelity. They typically rely on a separate reconstruction stage [31] to convert images into watertight shapes with accurate collisions and physical properties. The second paradigm performs explicit 3D generation, directly producing point clouds [52, 54, 56], meshes, or voxels. It depends on high-quality, curated 3D datasets [3, 32] and typically demands model designs [41, 42] that align with representation-specific properties (e.g., permutation invariance for point clouds, connectivity constraints for meshes, and spatial sparsity for voxels). However, many real-world objects are articulated, coupling geometry with kinematics; this setting stresses both paradigms and motivates dedicated

generative models for articulated shapes.

Within this articulated setting, interest is rising, but generative methods remain in their early stages. Most prior work focuses on analysis, such as part segmentation, articulation inference, and motion estimation [21, 22]. The challenge is to ensure 3D consistency, along with kinematic correctness and plausible deformation. Existing approaches either condition on a given image [5, 25] and then reconstruct its articulation, or they follow a multi-stage pipeline that first generates a kinematic graph (parts, joints, parameters) and subsequently synthesizes geometry for each part [26].

Against this backdrop, we propose a self-contained, 3D-explicit solution for articulated mechanism generation. We represent each object as a deformable point cloud and learn an action conditioned flow matching velocity field that captures kinematic motion from sets of deformation samples. We further condition the field on a shape prior, enabling a single model to capture the kinematics of an entire category of articulated shapes. By interpolating in the action and shape-prior space, the model generates novel instances and motions while maintaining 3D consistency and kinematic validity. As shown in Figure 1, we evaluate across multiple categories from the *PartNet-Mobility* [53] dataset and on simulated robots from *MuJoCo Menagerie* [49]. Our model exhibits disentangled conditioning: with the *shape prior* held fixed, generated samples preserve appearance while producing kinematically correct deformations; with the *action* held fixed, generated samples maintain a similar pose while varying appearance to yield novel instances.

Beyond visual novelty, these results point to a broader opportunity: the potential to address the long-standing scarcity of diverse robot morphologies. High quality articulated objects and simulation ready robot models are expensive. For example, *PartNet-Mobility* includes 26 folding chairs, and only 17 robot arms are available in *MuJoCo Menagerie*. Meanwhile, robot behavior datasets have scaled from RT-1 to RT-X [2, 38, 57], reaching 10^5 tasks with millions of trajectories, yet the number of distinct robot embodiments is 22, creating a morphology bottleneck. Viewing robots as autonomous articulated bodies, we explore whether generative models can produce novel embodiments with valid kinematics and meaningful morphology.

Our contributions: **(1)** We introduce an action conditioned flow matching framework that learns a velocity field in point space to generate deformations under given joint commands. **(2)** We extend the framework with joint conditioning on action and shape prior, enabling a single model to cover a category of articulated shapes and generate unseen instances with kinematically valid deformations. **(3)** We evaluate on everyday objects and robots, demonstrating controllable generation, interpolation across instances, and accurate kinematic behavior under novel action sequences.

Method	Model	Shape Generation	Latent Interpolation	Articulated Deformation	Color Support
VSM [4]	DeepSDF	✗	✗	✓	✗
FFKSM [15]	NeRF	✗	✗	✓	✗
l-GAN [1]	GAN	✓	✓	✗	✗
PointFlow [54]	CNF	✓	✓	✗	✗
PVD [56]	Diffusion	✓	✗	✗	✗
Point-E [35]	Diffusion	✓	✗	✗	✓
PSF [52]	Flow Matching	✓	✗	✗	✗
ArticFlow	Flow Matching	✓	✓	✓	✓

Table 1. **Compare with previous methods.** Rows 1–2 are neural simulation methods. Rows 3–7 are point cloud generation models.

2. Related Work

2.1. Point cloud generation

Early methods adapted GAN and VAE to unordered point sets, for example, l-GAN [1] and hierarchical set-structured Set-VAE [18]. Flow based approaches model continuous deformations in data space: PointFlow [54] learns a continuous normalizing flow over point clouds (trained on ShapeNet) by coupling a latent prior with a point-space flow. Diffusion models followed, including point-voxel or pure point formulations such as PVD [56], PSF [52], and DiT-3D [33], which leverage score driven denoising with set-aware backbones. Latent diffusion has also been explored: LION [50] trains an autoencoder for point sets and performs diffusion in the learned latent. Beyond unconditional generation, Point-E [35] conditions on 2D image priors or text to produce colored point clouds, while the autoregressive tokenization of point sets (e.g., PointGPT [6]) treats generation as next-token prediction with permutation-robust tokenizers. These methods improve fidelity and diversity while addressing set invariance, geometric realism, and efficient editing and inpainting.

As generative models have grown in capability, architectural design has evolved from two-stage conditional generation, as in l-GAN and PointFlow, to direct one-stage formulations, such as the DDPM-based PVD and the rectified flow-matching framework of PSF.

2.2. Articulated object modeling and generation

Articulated objects are central to everyday tools and robotic manipulation, and interest is growing in both vision and robotics. Most prior work targets modeling and analysis: recovering parts, joints, and motion from images or 3D observations [24, 28, 34, 51]. Examples include Multi-BodySync [16], which segments rigid parts from point cloud sequences, and interaction-driven methods such as Ditto [17] and Structure-from-Action [36] that infer articulation parameters from robot interactions. Recent efforts translate perception into executable robot descriptions (Real2Code, URDFormer) [8, 30], and extend to complex robot structures (Watch-It-Move, AutoURDF) [22, 37].

Generative approaches are only beginning to be explored. Image-conditioned pipelines synthesize articulated geometry from a single view [5, 25]; mesh based methods deform or animate meshes with explicit part structures and joints [12, 43]; and graph based frameworks generate kinematic graphs before geometry [20, 26]. These methods are often influenced by visual priors and guided by geometric assumptions (e.g., mesh connectivity), which may limit their flexibility in representing diverse or free-form geometries. They often struggle to interpolate smoothly across instances and generate natural curved surfaces. By contrast, our method is self-contained and trained end-to-end; free form point cloud generation further enables smooth shape interpolations. Another related direction is *neural robot simulation* [4, 15], which learns task agnostic kinematic models from deformation samples in a differentiable form. However, prior works typically validate on one or a few specific robots, whereas our model captures a category of robots and generalizes to novel morphologies.

As task complexity rises for articulated mechanism generation, we revisit and adopt the two-stage design with flow matching to disentangle *shape* and *action*. Conditioned only on actions, our method functions as a neural simulator, predicting kinematically valid deformations of a given instance; conditioned only on a shape prior, it naturally generates diverse appearances while preserving the underlying kinematic functionality.

3. Method

3.1. Notation and Overview.

3D point-cloud generation aims to learn the sampling of permutation-invariant point sets from the data distribution. Methods based on diffusion and flow matching learn a mapping from a prior distribution P_0 , typically Gaussian noise $\mathcal{N}(0, I)$, to the data distribution, denoted as P_{data} . In this paper, we study action-conditioned flow matching that transports samples from a Gaussian prior to the shapes of articulated rigid bodies.

Given a dataset consisting of K sample pairs: point clouds $\mathcal{X} = \{X^i \in \mathbb{R}^{N \times 3}\}_{i=1}^K$ and action vectors $\mathcal{A} = \{A^i \in \mathbb{R}^J\}_{i=1}^K$, we jointly optimize two flow models. The point flow transports data in point-cloud space from the Gaussian prior $p_0 = \mathcal{N}(0, I_{N \times 3})$ to the target set \mathcal{X} . The latent flow transports vectors from the normal distribution $q_0 = \mathcal{N}(0, I_D)$ to the encoded latent-vector space $\mathcal{Z} = \{Z^i \in \mathbb{R}^D\}_{i=1}^K$. Here N is the number of points, J is the number of joints, and D is the dimension of the latent vector. We denote the point flow as $u_\theta(X_t, t | Z_a, Z_x)$ and the latent flow as $v_\psi(y_t, t | Z_a)$, where the encoded action latent is $Z_a = E_a(A)$ and the encoded point-cloud latent is $Z_x = E_x(X)$. For clarity of notation, we denote the pairwise (conditional) target velocities as u_t and v_t , the corre-

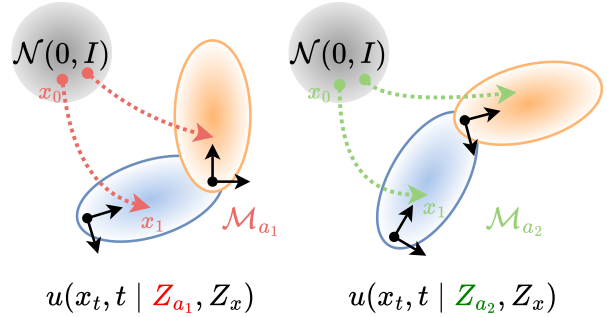


Figure 2. **Action-conditioned velocity fields.** With the shape prior Z_x fixed, changing the action embedding from Z_{a_1} (left) to Z_{a_2} (right) modulates the velocity fields $v(x, t | Z_a, Z_x)$. Each field transports states from the Gaussian prior ($x_0 \sim \mathcal{N}(0, I)$) to an action-specific manifold \mathcal{M}_a along the path x_t , producing distinct kinematic deformations. In our case, the target manifold consists of articulated rigid bodies represented as point clouds.

sponding marginal (expected) ground-truth velocities as u^* and v^* , and the learnable velocity networks as u_θ and v_ψ .

In summary, the point flow learns the velocity field of the point cloud under the action and shape-prior conditions, and the latent flow learns to generate the shape-prior vector. We use point clouds \mathcal{X} and action vectors \mathcal{A} to train these two flow models. The goal is to train both flow models so that we can generate novel point clouds \hat{X} that follow the action condition \hat{A} with kinematically consistent deformations.

3.2. Action conditioned flow

Flow Matching derives from the framework of Neural Ordinary Differential Equations (Neural ODEs) [7], where a data sample is obtained by integrating a continuous-time velocity field. Instead of directly fitting the ODE trajectory to data, Flow Matching learns the instantaneous velocity field that transports samples from a prior distribution to the data distribution. Intuitively, during training, each data pair (X_0, X_1) defines a straight-line path $X_t = (1-t)X_0 + tX_1$ and an associated velocity $X_1 - X_0$. By minimizing the discrepancy between predicted and target velocities over random time steps and pairings, the network gradually converges to the *marginal velocity field*, which represents the expected instantaneous transport direction at any intermediate state. This marginal field defines a continuous flow that can be integrated as an ODE to generate samples from the learned distribution.

We now instantiate Flow Matching in point space by conditioning the velocity field on the joint action. Given the encoded action latent $Z_a = E_a(A)$, the point flow aims to learn a velocity field $u_\theta(X_t, t | Z_a)$ that transports samples from the Gaussian prior to the articulated shapes in data space. As the given X_t may correspond to multiple

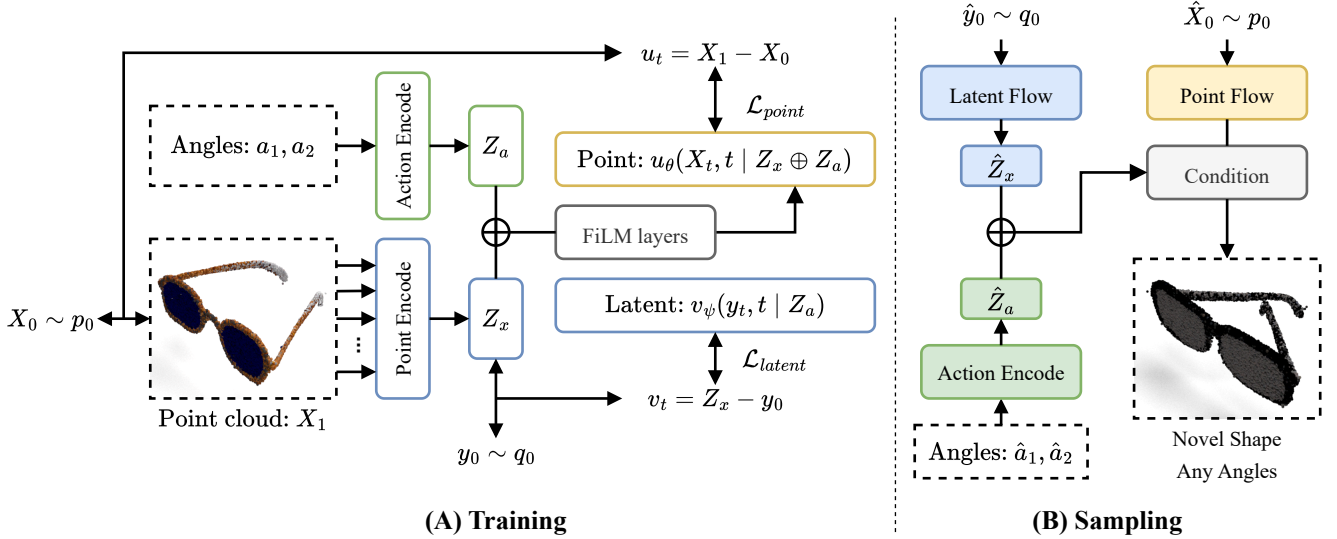


Figure 3. **Two-stage conditioned flow matching.** (A). For each training pair (X_1, A) , we encode the point cloud with PointNet [41] to obtain the shape latent code Z_x and encode the joint angles (Fourier layers [48] + MLP) to obtain Z_a . We jointly optimize two flow-matching models: The *point flow* u_θ predicts a conditional velocity in point space that transports points from a prior p_0 to the target set X_1 using straight-line pairings (target point set velocity $X_1 - X_0$). The concatenated condition $(Z_x \oplus Z_a)$, added with time embedding, is injected using FiLM [40] layers. The *latent flow* v_ψ transports latent noise y_0 to the shape code Z_x , with target velocity $Z_x - y_0$. (B). At sampling time, We first draw latent noise $\hat{y}_0 \sim q_0$ and an action set (\hat{a}_1, \hat{a}_2) . Integrating the latent ODE $\dot{y}_t = v_\psi$ forward from $t=0$ to $t=1$ yields a sampled shape latent code \hat{Z}_x . We then form the condition with \hat{Z}_x and \hat{Z}_a , draw a point prior $\hat{X}_0 \sim p_0$, and integrate the point ODE $\dot{X}_t = u_\theta$ to obtain the generated point cloud \hat{X} . This produces novel shapes with controllable articulation under arbitrary actions.

(X_0, X_1) pairs, we learn the *marginal velocity*:

$$u^*(X, t | Z_a) = \mathbb{E}[u_t | X_t = X, t, Z_a] \quad (1)$$

which represents the expected instantaneous velocity of a point set conditioned on action. The *conditional velocity* $u_t = X_1 - X_0$. The flow matching loss minimizes the squared error between the network prediction and the target velocity:

$$\mathcal{L}_{\text{point}} = \mathbb{E}_{t, X_0, X_1} \left[\|u_\theta(X_t, t | Z_a) - u_t\|_2^2 \right]. \quad (2)$$

Here t is sampled from a time distribution (e.g., Beta(2, 1)) and $X_t = (1 - t)X_0 + tX_1$ is the interpolated point set. After training, new samples are generated by solving the ODE

$$\dot{X}_t = u_\theta(X_t, t | Z_a), \quad \hat{X}_0 \sim p_0 \quad (3)$$

which evolves the initial noise \hat{X}_0 toward a valid articulated shape \hat{X} under the action code Z_a . In practice, we apply numerical integration, such as Euler updates $X_{k+1} = X_k + h u_\theta(X_k, t_k | Z_a)$, where h denotes the step size.

3.3. Action and shape-prior conditioned flow

In the two-stage conditioned flow matching, as shown in Figure 3 (A), we jointly optimize two flow matching models. Equation 1 will be extended with two latent conditions:

$$u^*(X, t | Z_a, Z_x) = \mathbb{E}[u_t | X_t = X, t, Z_a, Z_x] \quad (4)$$

Here Z_x is the encoded shape latent vector, $E_x(X)$. We then introduce the second flow matching model v_ψ , along with the corresponding *marginal velocity* in latent space:

$$v^*(y, t | Z_a) = \mathbb{E}[v_t | y_t = y, t, Z_a] \quad (5)$$

We use straight-line pairings to define the conditional velocities. In point space, we sample $X_0 \sim p_0$ and $X_1 \sim p_{\text{data}}(\cdot | Z_a, Z_x)$, construct the interpolated point set $X_t = (1 - t)X_0 + tX_1$, and define the pairwise velocity $u_t = X_1 - X_0$. Similarly, in latent space, we sample $y_0 \sim q_0$, set $y_t = (1 - t)y_0 + tZ_x$, and define $v_t = Z_x - y_0$. As shown in algorithm 1, we use a time sampling distribution, typically Beta(2, 1), which places higher density near $t = 1$ and improves training stability in the later steps of the flow.

In our implementation, the shape latent Z_x and the action latent Z_a are designed to have the same dimensionality as time embedding, so we can combine them by elementwise addition, which is then passed through FiLM layers[40]. The FiLM module generates feature-wise scale and shift parameters, allowing the condition to modulate intermediate activations of the velocity networks through affine transformations. This provides an efficient and expressive way to inject both shape and action information into the flow-matching models without altering their core architectures.

Generally, this two stage design factorizes shape and action into two independent latent spaces. The latent flow v_ψ

learns a distribution over shape codes by transporting noise toward the encoded vectors Z_x , effectively compressing geometric variability into a compact latent prior. Conditioned on a sampled shape code, the point flow u_θ focuses solely on action driven deformation, learning how each instance moves under different joint commands. This separation allows us to first generate a plausible shape latent that matches the data distribution and then apply the action conditioned point flow to produce articulated motions with disentangled control over shape and action.

3.4. Sampling and Interpolation

At sampling time (Figure 3 (B) and Algorithm 2), we first command an input action \hat{A} and encode it into a latent vector $\hat{Z}_a = E_a(\hat{A})$. We then sample latent noise and integrate the latent flow ODE to obtain a shape code:

$$\dot{y}_t = v_\psi(y_t, t \mid \hat{Z}_a) \quad (6)$$

with $y_0 \sim q_0$, $\hat{Z}_x = y_1$. Given this integrated shape latent \hat{Z}_x and the action latent \hat{Z}_a , we initialize a point cloud and integrate the point flow ODE:

$$\dot{X}_t = u_\theta(X_t, t \mid \hat{Z}_x, \hat{Z}_a) \quad (7)$$

with $X_0 \sim p_0$, $\hat{X} = X_1$. This equation yields a novel articulated shape \hat{X} consistent with the conditioned shape and action. In practice, both ODEs are solved numerically using Heun’s method (improved Euler) with S_{lat} and S_{pt} integration steps for the latent and point flows, respectively. The detailed calculation steps are specified in the algorithm block. In general, the sampling framework takes only the joint conditions as input. Given the trained flow models v_ψ and u_θ , it generates new objects whose articulation follows the commanded joint configurations.

For interpolation, we simply perform spherical linear interpolation (slerp) in the shape latent space. Given two sampled shape latents $\hat{Z}_x^{(0)}$ and $\hat{Z}_x^{(1)}$, we generate intermediate latent codes $\hat{Z}_x(\alpha)$ with $\alpha \in [0, 1]$ by

$$\text{slerp}(\hat{Z}_x^{(0)}, \hat{Z}_x^{(1)}; \alpha) = \frac{\sin((1-\alpha)\phi)}{\sin\phi} \hat{Z}_x^{(0)} + \frac{\sin(\alpha\phi)}{\sin\phi} \hat{Z}_x^{(1)}$$

where ϕ represents the angle between the two latent vectors $\hat{Z}_x^{(0)}$ and $\hat{Z}_x^{(1)}$, which is the geodesic distance on the unit hypersphere connecting their normalized directions.

Unlike static point cloud generation work on large datasets such as ShapeNet [3], PartNet-Mobility [53] provides limited instances per category. Although we wish for the latent shape to capture kinematics-irrelevant features, learning a meaningful latent space with limited samples is challenging. We therefore validate two variants. First, we condition the shape latent flow on both the category shape and the action deformation by injecting the action latent \hat{Z}_a .

Algorithm 1 ArticFlow Training (Flow Matching)

Require: Dataset $\{(X^i, A^i)\}_{i=1}^K$
priors $p_0 = \mathcal{N}(0, I_{N \times 3})$, $q_0 = \mathcal{N}(0, I_D)$
velocity fields u_θ, v_ψ , optimizer Opt.

- 1: **for** step = 1 to T **do**
- 2: Sample minibatch X_1, A
- 3: $Z_x \leftarrow E_x(X_1)$, $Z_a \leftarrow E_a(A)$ ▷ Encode
- 4: Sample $t_x \sim \text{Beta}(2, 1)$, $X_0 \sim p_0$ ▷ Point flow
- 5: $X_t \leftarrow (1 - t_x) X_0 + t_x X_1$
- 6: $u_t \leftarrow X_1 - X_0$, $u \leftarrow u_\theta(X_t, t \mid Z_x, Z_a)$
- 7: $\mathcal{L}_{\text{point}} \leftarrow \text{MSE}(u, u_t)$
- 8: Sample $t_z \sim \text{Beta}(2, 1)$, $y_0 \sim q_0$ ▷ Latent flow
- 9: $y_t \leftarrow (1 - t_z) y_0 + t_z Z_x$
- 10: $v_t \leftarrow Z_x - y_0$, $v \leftarrow v_\psi(y_t, t \mid Z_a)$
- 11: $\mathcal{L}_{\text{latent}} \leftarrow \text{MSE}(v, v_t)$
- 12: $\mathcal{L} \leftarrow \mathcal{L}_{\text{point}} + \lambda \mathcal{L}_{\text{latent}}$
- 13: Opt.step() ▷ Optimize $E_x, E_a, u_\theta, v_\psi$
- 14: **end for**

Algorithm 2 ArticFlow Sampling (Heun RK2)

Require: Trained v_ψ, u_θ , encoder E_a , action \hat{A}
priors $q_0 = \mathcal{N}(0, I_D)$, $p_0 = \mathcal{N}(0, I_{N \times 3})$
steps $S_{\text{lat}}, S_{\text{pt}}$

- 1: **procedure** HEUN(field, x_0 , cond, S) ▷ Improved Euler
- 2: $h \leftarrow 1/S$; $x \leftarrow x_0$; $t \leftarrow 0$
- 3: **for** $s = 1$ to S **do**
- 4: $k_1 \leftarrow \text{field}(x, t \mid \text{cond})$
- 5: $\bar{x} \leftarrow x + h k_1$
- 6: $k_2 \leftarrow \text{field}(\bar{x}, t+h \mid \text{cond})$
- 7: $x \leftarrow x + \frac{h}{2}(k_1 + k_2)$; $t \leftarrow t + h$
- 8: **end for**
- 9: **return** x
- 10: **end procedure**
- 11: $\hat{Z}_a \leftarrow E_a(\hat{A})$
- 12: $\hat{Z}_x \leftarrow \text{HEUN}(v_\psi, y_0 \sim q_0, \hat{Z}_a, S_{\text{lat}})$
- 13: $\hat{X} \leftarrow \text{HEUN}(u_\theta, X_0 \sim p_0, \hat{Z}_x, \hat{Z}_a, S_{\text{pt}})$
- 14: **return** \hat{X}

The same as illustrated above. In the second version, we remove the action condition and train an unconditional shape latent flow with large shape diversity. In the later stage of training, we additionally attach a conditional adversarial module with a gradient reversal layer (GRL) [11] to remove action information from the shape latent. We compare these variants, denoted as ArticFlow (Cond-latent) and ArticFlow (Adv-latent), in the Experiments 4 section.

ArticFlow also supports colored point cloud generation by simply concatenating 3D positions and RGB values. Specifically, we extend the point flow velocity field to operate on 6D vectors and train it with input X_0 and target X_1 , both of which contain position and color channels.

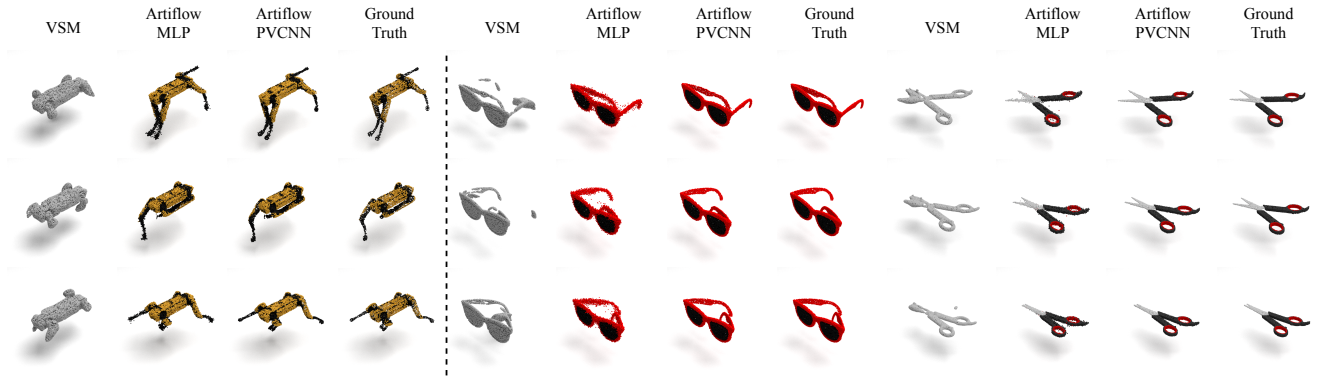


Figure 4. **Action-conditioned flow: qualitative results.** For a fixed object and varying joint actions, we compare the deformed point clouds predicted by VSM, ArticFlow-MLP, ArticFlow-PVCNN, and the ground truth. Conditioned only on the action latent, ArticFlow produces shapes whose articulation more closely matches the target kinematics than VSM.

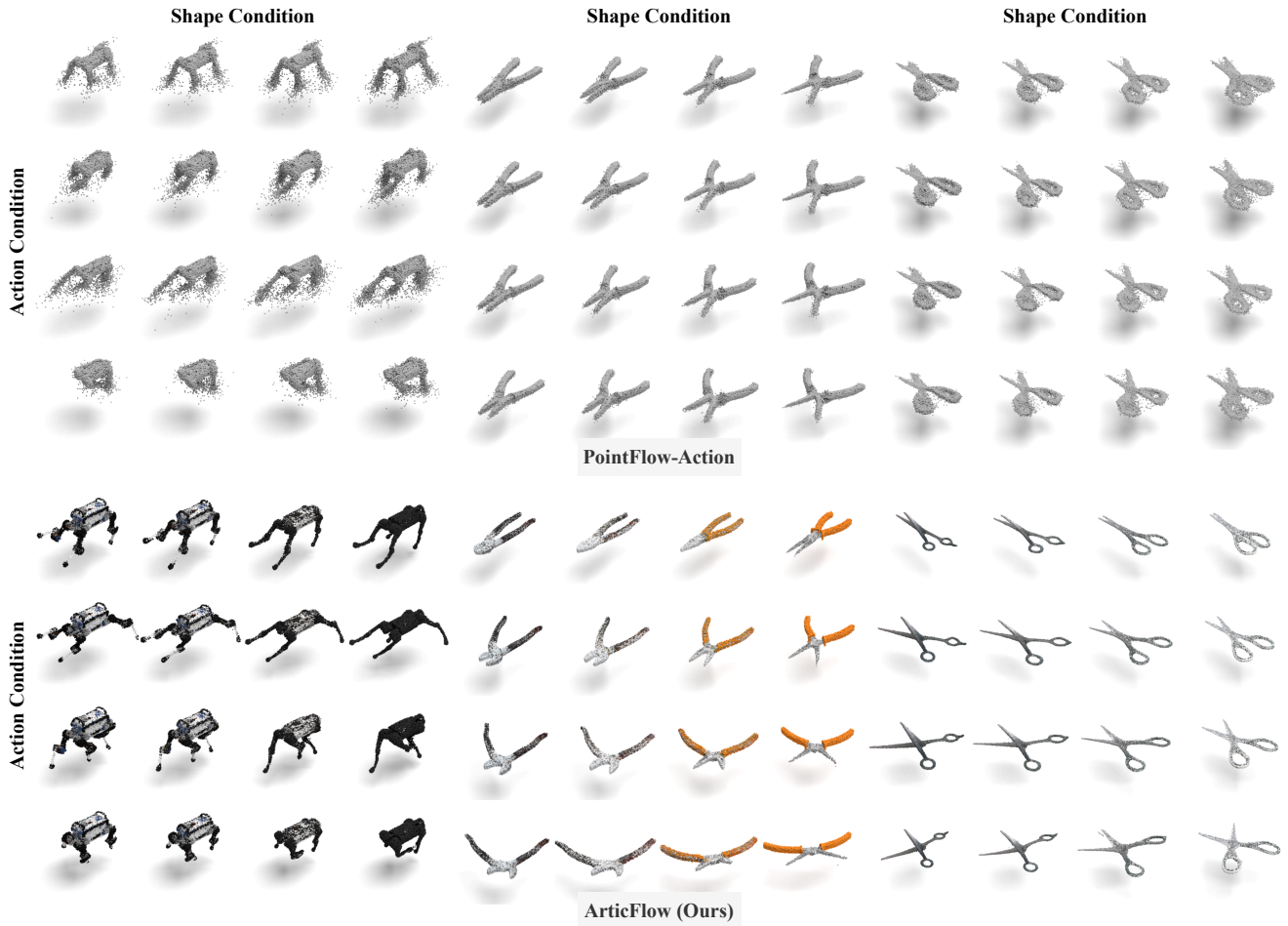


Figure 5. **Action and shape-prior conditioned flow, qualitative results.** When conditioned on both the shape latent and the action latent, we compare our method (ArticFlow) with the action-conditioned PointFlow baseline. Columns vary the shape prior (different object instances) and rows sweep the action condition. ArticFlow produces higher-quality surfaces and kinematically valid deformations. For the PointFlow-Action baseline, simple 1-DoF objects show only minor deformation across angle conditions, and more complex kinematics lose fine shape details, such as the robot legs.

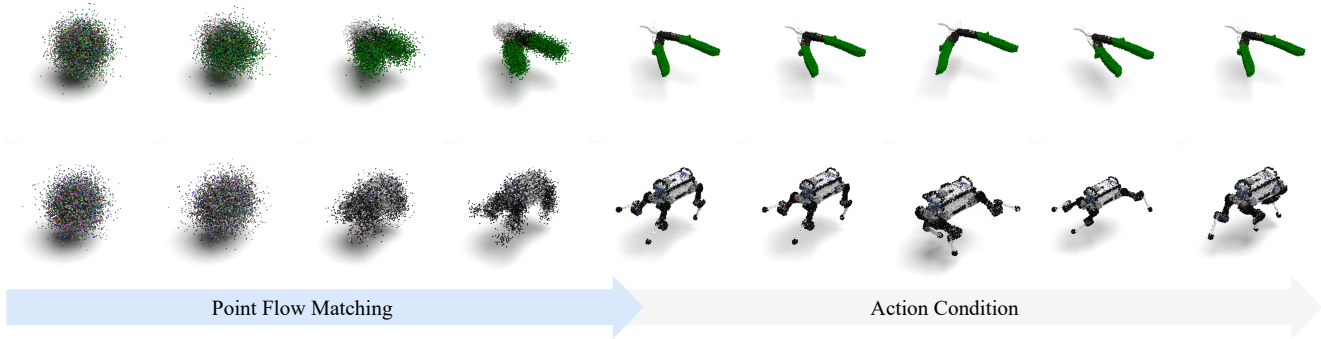


Figure 6. **Generation process and action conditioning.** Two examples from models trained on pliers (top) and quadruped robots (bottom). On the left, point flow matching transforms Gaussian noise into object shape; on the right, sampling random joint commands produces diverse articulated configurations of the same shape. Shape and color are generated jointly from 6D Gaussian prior.

4. Experiments

4.1. Dataset and Metrics

We validate our method on five categories: pliers, scissors, and eyeglasses from PartNet-Mobility, robot arms and quadrupeds from MuJoCo Menagerie. For each PartNet-Mobility object, we use 50 kinematic samples, and for each robot we use 1000 action configurations, with a 5:1 train–test split. For PartNet categories, each point cloud contains 20k points for flow training. For the robot categories, we use fewer points per sample, namely 4,096, since there are many more kinematic samples per object. We adopt these settings for all quantitative and qualitative experiments. During sampling and evaluation, we resample each prediction to 20k points so that all evaluation metrics are computed on point clouds of the same size. Within each category, the number of degrees of freedom (DoF) can vary across instances; therefore, we pad the action vectors with zeros up to the maximum DoF in that category. For complex structures such as robots, the rotation directions along the kinematic tree may differ between models; before training, we normalize all joint rotations by aligning them to the Denavit–Hartenberg (DH) convention for the robot dataset.

The goal of our quantitative experiments is to evaluate whether ArticFlow can produce kinematically correct shapes and how accurately it follows the commanded joint actions. Direct evaluation of novel articulated shapes is difficult, since ground-truth deformations for unseen objects are not available. Therefore, we measure kinematic accuracy on latent codes decoded from articulated objects in the dataset, conditioning on unseen action configurations. We compare ArticFlow with the action-conditioned PointFlow baseline. We also consider a single-object setting, where the model is trained on one specific robot and conditioned only on the action, and compare it with the visual self-modeling [4] (VSM) method designed for robot representation learning.

For evaluation, we use both the L2-Chamfer Distance (CD) and the Earth Mover’s Distance (EMD) between the predicted and ground-truth point clouds. Chamfer captures overall shape similarity and is efficient to compute, while EMD provides a transport based measure that is more sensitive to local misalignment. Reporting both metrics provides a more complete assessment of geometric accuracy.

4.2. Qualitative Results

For baseline comparison, we adapt the original PointFlow [54] model into an action-conditioned generator by injecting the action information through FiLM layers while keeping the CNF-based training framework, denoted as PointFlow-Action. To compare fairly with VSM, which requires high-quality surface normals, we additionally implement its training pipeline and construct a dedicated dataset: starting from the same point clouds used by ArticFlow, we reconstruct watertight meshes and compute normals before training VSM. Figure 4 shows qualitative results for the action conditioned setting. For a fixed object and varying joint actions, ArticFlow produces deformations that more closely follow the target kinematics than VSM, especially in thin structures such as eyeglass legs and robot limbs. Between our two backbones, the PVCNN [29] variant yields sharper and more complete surfaces than the per-point MLP. Figure 5 presents qualitative results for joint shape and action conditioned generation. Compared with the action conditioned PointFlow baseline, ArticFlow generates higher-quality surfaces and more kinematically consistent deformations across different instances within each category. In addition, ArticFlow naturally supports color generation, whereas VSM and PointFlow do not capture RGB features.

4.3. Quantitative Results

In the action condition setting (Table 2), ArticFlow substantially outperforms VSM across categories in CD and EMD, indicating more accurate kinematic deformation for appear-

Simulation	CD ↓					EMD ↓				
	Arms	Quadrupeds	Pliers	Scissors	Eyeglasses	Arms	Quadrupeds	Pliers	Scissors	Eyeglasses
VSM [4]	12.4763	14.5676	0.0527	1.7208	10.7652	57.7256	66.9668	8.7149	45.9159	76.1755
ArticFlow(MLP)	0.0599	0.1853	0.1232	0.0780	0.1522	20.9800	15.9860	14.9094	14.6320	29.1480
ArticFlow(PVCNN)	0.6228	0.1675	0.1240	0.0481	0.1400	11.1780	5.8883	9.9892	8.5441	4.4339

Table 2. **Baseline comparison on action-conditioned simulation.** Chamfer Distance (CD) and Earth Move Distance (EMD) values $\times 10^3$.

Generation	CD ↓					EMD ↓				
	Arms	Quadrupeds	Pliers	Scissors	Eyeglasses	Arms	Quadrupeds	Pliers	Scissors	Eyeglasses
PointFlow-Action	0.2824	1.4416	0.3591	0.4829	1.8308	62.8441	79.5037	73.3096	76.0229	182.6917
ArticFlow(Uncond-latent)	0.6061	0.2502	0.0281	0.0308	0.0207	16.8010	8.2525	4.4291	6.0803	4.3361
ArticFlow(Cond-latent)	0.6776	0.2651	0.0281	0.0295	0.0366	18.2628	8.7380	4.5394	6.2370	4.2984
ArticFlow(Adv-latent)	0.0616	0.2194	0.0306	0.0361	0.0311	9.8705	7.9411	4.6393	6.4390	3.6163

Table 3. **Baseline comparison on action and shape-prior conditioned generation.** CD and EMD values $\times 10^3$.

ance fixed objects. Comparing backbones, the PVCNN variant consistently improves upon the per-point MLP architecture, especially in EMD, suggesting that the point-convolution module captures local geometric structure more effectively and therefore reduces the transport cost between the predicted and ground-truth point sets.

In the two stage generation setting (Table 3), all ArticFlow variants outperform the action-conditioned PointFlow baseline, showing that our joint shape–action modeling yields more accurate articulated shapes. The different latent-flow designs achieve similar CD and EMD, with the unconditional latent and the adversarially regularized latent performing slightly better overall, indicating that discouraging kinematic information in the shape latent can improve generalization.

4.4. Applications and Future Work

Figures 6 and 7 illustrate that ArticFlow supports both generation and simulation oriented reconstruction. Figure 6 shows how our point-flow first maps 6D Gaussian noise to a canonical colored shape and then uses action conditioning to produce diverse articulated configurations. Figure 7 demonstrates that these generated point clouds can be converted into high-quality watertight meshes using recent point cloud to mesh work [55]. Bridging with popular articulation modeling methods, ArticFlow outputs could be further transformed into simulation-ready description files (e.g., URDF), closing the loop towards fully generated, simulation-ready articulated models.

5. Discussion

Limitations. Our approach also has several limitations. First, generation is currently limited to the categories and articulation patterns present in the training datasets; extend-

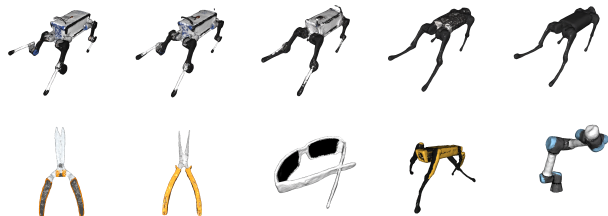


Figure 7. **Point cloud to mesh.** We demonstrate interpolated point clouds from ArticFlow and their conversion to watertight meshes. The top row shows an interpolation sequence between two legged robots. The bottom row presents random samples from other categories. We preserve the color from point cloud to mesh.

ing to more diverse objects would require additional curated data. Second, joint directions and ranges must be aligned for high-quality training, which limits our ability to directly learn from real-world articulated data. Finally, while the model can be queried with actions outside the training range, such extrapolated poses may yield unrealistic geometries.

Conclusion. This paper shows that action-conditioned flow matching provides an effective framework for controllable articulated 3D generation. ArticFlow combines a latent flow for shape priors with a point flow for action-conditioned deformations, allowing a single model to represent diverse articulated categories and generalize across actions. In both PartNet-Mobility and MuJoCo Menagerie experiments, ArticFlow outperforms the action-conditioned PointFlow and VSM in terms of deformation accuracy. We expect this framework to scale to broader object categories and to integrate with simulation-ready description formats in future work.

References

- [1] Panos Achlioptas, Olga Diamanti, Ioannis Mitliagkas, and Leonidas Guibas. Learning representations and generative models for 3d point clouds. In *International conference on machine learning*, pages 40–49. PMLR, 2018. 2
- [2] Anthony Brohan, Noah Brown, Justice Carbajal, Yevgen Chebotar, Joseph Dabis, Chelsea Finn, Keerthana Gopalakrishnan, Karol Hausman, Alex Herzog, Jasmine Hsu, et al. Rt-1: Robotics transformer for real-world control at scale. *arXiv preprint arXiv:2212.06817*, 2022. 2
- [3] Angel X Chang, Thomas Funkhouser, Leonidas Guibas, Pat Hanrahan, Qixing Huang, Zimo Li, Silvio Savarese, Manolis Savva, Shuran Song, Hao Su, et al. Shapenet: An information-rich 3d model repository. *arXiv preprint arXiv:1512.03012*, 2015. 1, 5
- [4] Boyuan Chen, Robert Kwiatkowski, Carl Vondrick, and Hod Lipson. Fully body visual self-modeling of robot morphologies. *Science Robotics*, 7(68):eabn1944, 2022. 2, 3, 7, 8
- [5] Chuhan Chen, Isabella Liu, Xinyue Wei, Hao Su, and Minghua Liu. Freart3d: Training-free articulated object generation using 3d diffusion. *arXiv preprint arXiv:2510.25765*, 2025. 2, 3
- [6] Guangyan Chen, Meiling Wang, Yi Yang, Kai Yu, Li Yuan, and Yufeng Yue. Pointgpt: Auto-regressively generative pre-training from point clouds. *Advances in Neural Information Processing Systems*, 36:29667–29679, 2023. 2
- [7] Ricky TQ Chen, Yulia Rubanova, Jesse Bettencourt, and David K Duvenaud. Neural ordinary differential equations. *Advances in neural information processing systems*, 31, 2018. 3
- [8] Zoey Chen, Aaron Walsman, Marius Memmel, Kaichun Mo, Alex Fang, Karthikeya Vemuri, Alan Wu, Dieter Fox, and Abhishek Gupta. Urdformer: A pipeline for constructing articulated simulation environments from real-world images. *arXiv preprint arXiv:2405.11656*, 2024. 2
- [9] Matt Deitke, Ruoshi Liu, Matthew Wallingford, Huong Ngo, Oscar Michel, Aditya Kusupati, Alan Fan, Christian Laforte, Vikram Voleti, Samir Yitzhak Gadre, et al. Objaverse-xl: A universe of 10m+ 3d objects. *Advances in Neural Information Processing Systems*, 36:35799–35813, 2023. 1
- [10] Matt Deitke, Dustin Schwenk, Jordi Salvador, Luca Weihs, Oscar Michel, Eli VanderBilt, Ludwig Schmidt, Kiana Ehsani, Aniruddha Kembhavi, and Ali Farhadi. Objaverse: A universe of annotated 3d objects. In *Proceedings of the IEEE/CVF conference on computer vision and pattern recognition*, pages 13142–13153, 2023. 1
- [11] Yaroslav Ganin, Evgeniya Ustinova, Hana Ajakan, Pascal Germain, Hugo Larochelle, François Laviolette, Mario March, and Victor Lempitsky. Domain-adversarial training of neural networks. *Journal of machine learning research*, 17(59):1–35, 2016. 5
- [12] Daoyi Gao, Yawar Siddiqui, Lei Li, and Angela Dai. Meshart: Generating articulated meshes with structure-guided transformers. In *Proceedings of the Computer Vision and Pattern Recognition Conference*, 2025. 3
- [13] Ian J Goodfellow, Jean Pouget-Abadie, Mehdi Mirza, Bing Xu, David Warde-Farley, Sherjil Ozair, Aaron Courville, and Yoshua Bengio. Generative adversarial nets. *Advances in neural information processing systems*, 27, 2014. 1
- [14] Jonathan Ho, Ajay Jain, and Pieter Abbeel. Denoising diffusion probabilistic models. *Advances in neural information processing systems*, 33:6840–6851, 2020. 1
- [15] Yuhang Hu, Jiong Lin, and Hod Lipson. Teaching robots to build simulations of themselves. *Nature Machine Intelligence*, pages 1–11, 2025. 2, 3
- [16] Jiahui Huang, He Wang, Tolga Birdal, Minhyuk Sung, Federica Arrigoni, Shi-Min Hu, and Leonidas J Guibas. Multibodysync: Multi-body segmentation and motion estimation via 3d scan synchronization. In *Proceedings of the IEEE/CVF Conference on Computer Vision and Pattern Recognition*, pages 7108–7118, 2021. 2
- [17] Zhenyu Jiang, Cheng-Chun Hsu, and Yuke Zhu. Ditto: Building digital twins of articulated objects from interaction. In *Proceedings of the IEEE/CVF Conference on Computer Vision and Pattern Recognition*, pages 5616–5626, 2022. 2
- [18] Jinwoo Kim, Jaehoon Yoo, Juho Lee, and Seunghoon Hong. Setvae: Learning hierarchical composition for generative modeling of set-structured data. In *Proceedings of the IEEE/CVF Conference on Computer Vision and Pattern Recognition*, pages 15059–15068, 2021. 2
- [19] Diederik P Kingma and Max Welling. Auto-encoding variational bayes. *arXiv preprint arXiv:1312.6114*, 2013. 1
- [20] Jiahui Lei, Congyue Deng, Bokui Shen, Leonidas Guibas, and Kostas Daniilidis. Nap: Neural 3d articulation prior. *arXiv preprint arXiv:2305.16315*, 2023. 3
- [21] Xiaolong Li, He Wang, Li Yi, Leonidas J Guibas, A Lynn Abbott, and Shuran Song. Category-level articulated object pose estimation. In *Proceedings of the IEEE/CVF conference on computer vision and pattern recognition*, pages 3706–3715, 2020. 2
- [22] Jiong Lin, Lechen Zhang, Kwansoo Lee, Jialong Ning, Judah Goldfeder, and Hod Lipson. Autourdf: Unsupervised robot modeling from point cloud frames using cluster registration. In *Proceedings of the Computer Vision and Pattern Recognition Conference*, pages 27628–27637, 2025. 2
- [23] Yaron Lipman, Ricky TQ Chen, Heli Ben-Hamu, Maximilian Nickel, and Matt Le. Flow matching for generative modeling. *arXiv preprint arXiv:2210.02747*, 2022. 1
- [24] Jiayi Liu, Ali Mahdavi-Amiri, and Manolis Savva. Paris: Part-level reconstruction and motion analysis for articulated objects. In *Proceedings of the IEEE/CVF International Conference on Computer Vision*, pages 352–363, 2023. 2
- [25] Jiayi Liu, Denys Iliash, Angel X Chang, Manolis Savva, and Ali Mahdavi-Amiri. Singapo: Single image controlled generation of articulated parts in objects. *arXiv preprint arXiv:2410.16499*, 2024. 2, 3
- [26] Jiayi Liu, Hou In Ivan Tam, Ali Mahdavi-Amiri, and Manolis Savva. Cage: Controllable articulation generation. In *Proceedings of the IEEE/CVF Conference on Computer Vision and Pattern Recognition*, pages 17880–17889, 2024. 2, 3
- [27] Ruoshi Liu, Rundi Wu, Basile Van Hoorick, Pavel Tokmakov, Sergey Zakharov, and Carl Vondrick. Zero-1-to-3: Zero-shot one image to 3d object. In *Proceedings of the IEEE/CVF international conference on computer vision*, pages 9298–9309, 2023. 1

- [28] Shaowei Liu, Saurabh Gupta, and Shenlong Wang. Building rearticulable models for arbitrary 3d objects from 4d point clouds. In *Proceedings of the IEEE/CVF Conference on Computer Vision and Pattern Recognition*, pages 21138–21147, 2023. 2
- [29] Zhijian Liu, Haotian Tang, Yujun Lin, and Song Han. Point-voxel cnn for efficient 3d deep learning. *Advances in neural information processing systems*, 32, 2019. 7
- [30] Zhao Mandi, Yijia Weng, Dominik Bauer, and Shuran Song. Real2code: Reconstruct articulated objects via code generation. *arXiv preprint arXiv:2406.08474*, 2024. 2
- [31] Ben Mildenhall, Pratul P Srinivasan, Matthew Tancik, Jonathan T Barron, Ravi Ramamoorthi, and Ren Ng. Nerf: Representing scenes as neural radiance fields for view synthesis. *Communications of the ACM*, 65(1):99–106, 2021. 1
- [32] Kaichun Mo, Shilin Zhu, Angel X Chang, Li Yi, Subarna Tripathi, Leonidas J Guibas, and Hao Su. Partnet: A large-scale benchmark for fine-grained and hierarchical part-level 3d object understanding. In *Proceedings of the IEEE/CVF conference on computer vision and pattern recognition*, pages 909–918, 2019. 1
- [33] Shentong Mo, Enze Xie, Ruihang Chu, Lanqing Hong, Matthias Niessner, and Zhenguo Li. Dit-3d: Exploring plain diffusion transformers for 3d shape generation. *Advances in neural information processing systems*, 36:67960–67971, 2023. 2
- [34] Jiteng Mu, Weichao Qiu, Adam Kortylewski, Alan Yuille, Nuno Vasconcelos, and Xiaolong Wang. A-sdf: Learning disentangled signed distance functions for articulated shape representation. In *Proceedings of the IEEE/CVF International Conference on Computer Vision*, pages 13001–13011, 2021. 2
- [35] Alex Nichol, Heewoo Jun, Prafulla Dhariwal, Pamela Mishkin, and Mark Chen. Point-e: A system for generating 3d point clouds from complex prompts. *arXiv preprint arXiv:2212.08751*, 2022. 2
- [36] Neil Nie, Samir Yitzhak Gadre, Kiana Ehsani, and Shuran Song. Structure from action: Learning interactions for articulated object 3d structure discovery. *arXiv preprint arXiv:2207.08997*, 2022. 2
- [37] Atsuhiko Noguchi, Umar Iqbal, Jonathan Tremblay, Tatsuya Harada, and Orazio Gallo. Watch it move: Unsupervised discovery of 3d joints for re-posing of articulated objects. In *Proceedings of the IEEE/CVF Conference on Computer Vision and Pattern Recognition*, pages 3677–3687, 2022. 2
- [38] Abby O’Neill, Abdul Rehman, Abhiram Maddukuri, Abhishek Gupta, Abhishek Padalkar, Abraham Lee, Acorn Pooley, Agrim Gupta, Ajay Mandelkar, Ajinkya Jain, et al. Open x-embodiment: Robotic learning datasets and rt-x models: Open x-embodiment collaboration 0. In *2024 IEEE International Conference on Robotics and Automation (ICRA)*, pages 6892–6903. IEEE, 2024. 2
- [39] George Papamakarios, Eric Nalisnick, Danilo Jimenez Rezende, Shakir Mohamed, and Balaji Lakshminarayanan. Normalizing flows for probabilistic modeling and inference. *Journal of Machine Learning Research*, 22(57):1–64, 2021. 1
- [40] Ethan Perez, Florian Strub, Harm De Vries, Vincent Dumoulin, and Aaron Courville. Film: Visual reasoning with a general conditioning layer. In *Proceedings of the AAAI conference on artificial intelligence*, 2018. 4
- [41] Charles R Qi, Hao Su, Kaichun Mo, and Leonidas J Guibas. Pointnet: Deep learning on point sets for 3d classification and segmentation. In *Proceedings of the IEEE conference on computer vision and pattern recognition*, pages 652–660, 2017. 1, 4
- [42] Charles Ruizhongtai Qi, Li Yi, Hao Su, and Leonidas J Guibas. Pointnet++: Deep hierarchical feature learning on point sets in a metric space. *Advances in neural information processing systems*, 30, 2017. 1
- [43] Xiaowen Qiu, Jincheng Yang, Yian Wang, Zhehuan Chen, Yufei Wang, Tsun-Hsuan Wang, Zhou Xian, and Chuang Gan. Articulate anymesh: Open-vocabulary 3d articulated objects modeling. *arXiv preprint arXiv:2502.02590*, 2025. 3
- [44] Danilo Rezende and Shakir Mohamed. Variational inference with normalizing flows. In *International conference on machine learning*, pages 1530–1538. PMLR, 2015. 1
- [45] Robin Rombach, Andreas Blattmann, Dominik Lorenz, Patrick Esser, and Björn Ommer. High-resolution image synthesis with latent diffusion models. In *Proceedings of the IEEE/CVF Conference on Computer Vision and Pattern Recognition (CVPR)*, pages 10684–10695, 2022. 1
- [46] Ruoxi Shi, Hansheng Chen, Zhuoyang Zhang, Minghua Liu, Chao Xu, Xinyue Wei, Linghao Chen, Chong Zeng, and Hao Su. Zero123++: a single image to consistent multi-view diffusion base model. *arXiv preprint arXiv:2310.15110*, 2023. 1
- [47] Jiaming Song, Chenlin Meng, and Stefano Ermon. Denoising diffusion implicit models. *arXiv preprint arXiv:2010.02502*, 2020. 1
- [48] Matthew Tancik, Pratul Srinivasan, Ben Mildenhall, Sara Fridovich-Keil, Nithin Raghavan, Utkarsh Singhal, Ravi Ramamoorthi, Jonathan Barron, and Ren Ng. Fourier features let networks learn high frequency functions in low dimensional domains. *Advances in neural information processing systems*, 33:7537–7547, 2020. 4
- [49] Yuval Tassa, Yotam Doron, Alistair Muldal, Tom Erez, Yazhe Li, Diego de Las Casas, David Budden, Abbas Abdolmaleki, Josh Merel, Andrew LeFrancq, et al. Deepmind control suite. *arXiv preprint arXiv:1801.00690*, 2018. 1, 2
- [50] Arash Vahdat, Francis Williams, Zan Gojcic, Or Litany, Sanja Fidler, Karsten Kreis, et al. Lion: Latent point diffusion models for 3d shape generation. *Advances in Neural Information Processing Systems*, 35:10021–10039, 2022. 2
- [51] Xiaogang Wang, Bin Zhou, Yahao Shi, Xiaowu Chen, Qingping Zhao, and Kai Xu. Shape2motion: Joint analysis of motion parts and attributes from 3d shapes. In *Proceedings of the IEEE/CVF Conference on Computer Vision and Pattern Recognition*, pages 8876–8884, 2019. 2
- [52] Lemeng Wu, Dilin Wang, Chengyue Gong, Xingchao Liu, Yunyang Xiong, Rakesh Ranjan, Raghuraman Krishnamoorthi, Vikas Chandra, and Qiang Liu. Fast point cloud generation with straight flows. In *Proceedings of the IEEE/CVF conference on computer vision and pattern recognition*, pages 9445–9454, 2023. 1, 2

- [53] Fanbo Xiang, Yuzhe Qin, Kaichun Mo, Yikuan Xia, Hao Zhu, Fangchen Liu, Minghua Liu, Hanxiao Jiang, Yifu Yuan, He Wang, et al. Sapien: A simulated part-based interactive environment. In *Proceedings of the IEEE/CVF conference on computer vision and pattern recognition*, pages 11097–11107, 2020. [1](#), [2](#), [5](#)
- [54] Guandao Yang, Xun Huang, Zekun Hao, Ming-Yu Liu, Serge Belongie, and Bharath Hariharan. Pointflow: 3d point cloud generation with continuous normalizing flows. In *Proceedings of the IEEE/CVF international conference on computer vision*, pages 4541–4550, 2019. [1](#), [2](#), [7](#)
- [55] Qiao Yu, Xianzhi Li, Yuan Tang, Xu Han, Jinfeng Xu, Long Hu, and Min Chen. Pointdreamer: Zero-shot 3d textured mesh reconstruction from colored point cloud. *IEEE Transactions on Visualization and Computer Graphics*, 2025. [8](#)
- [56] Linqi Zhou, Yilun Du, and Jiajun Wu. 3d shape generation and completion through point-voxel diffusion. In *Proceedings of the IEEE/CVF international conference on computer vision*, pages 5826–5835, 2021. [1](#), [2](#)
- [57] Brianna Zitkovich, Tianhe Yu, Sichun Xu, Peng Xu, Ted Xiao, Fei Xia, Jialin Wu, Paul Wohlhart, Stefan Welker, Ayzaan Wahid, et al. Rt-2: Vision-language-action models transfer web knowledge to robotic control. In *Conference on Robot Learning*, pages 2165–2183. PMLR, 2023. [2](#)

ArticFlow: Generative Simulation of Articulated Mechanisms

Supplementary Material

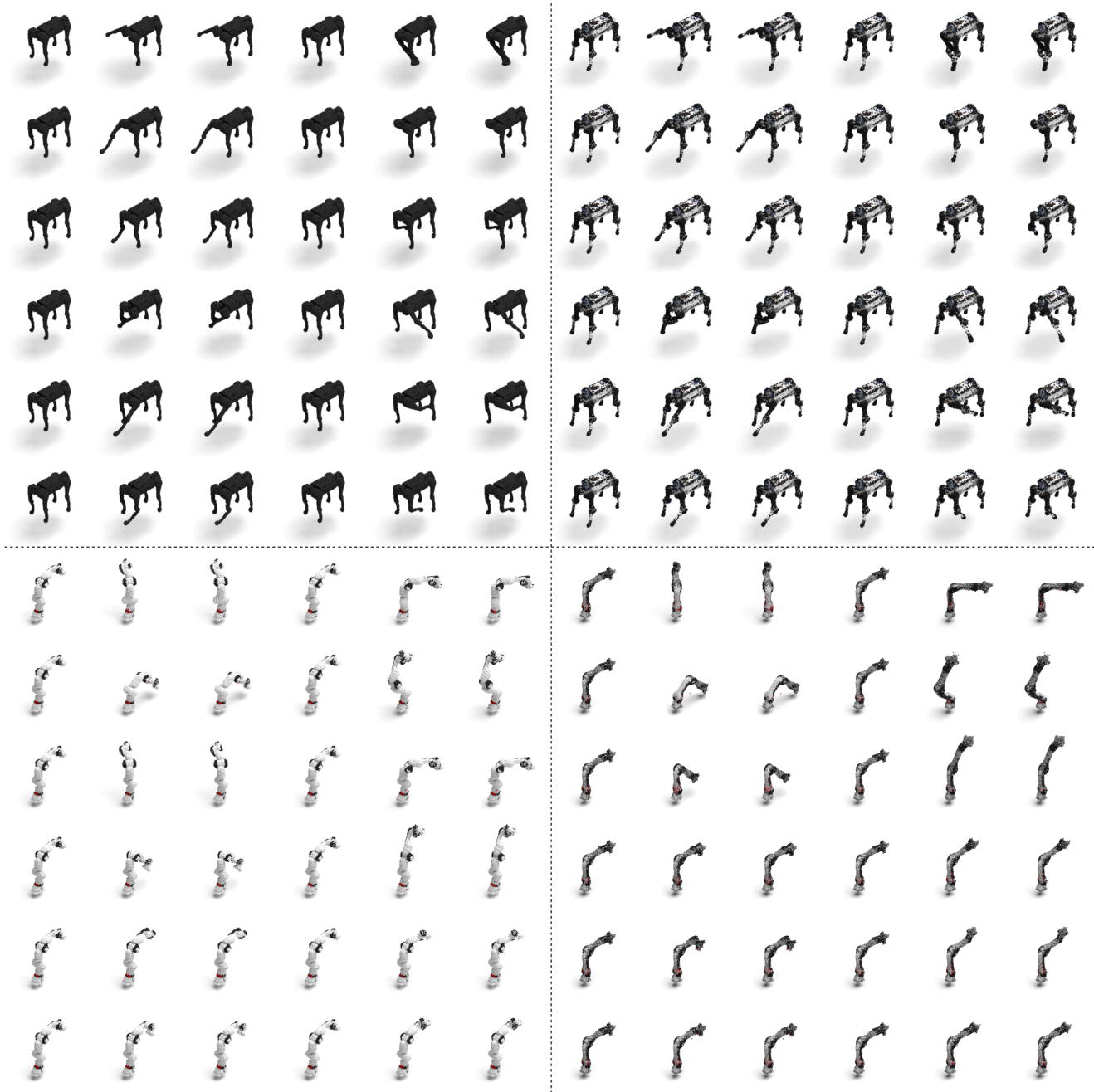


Figure 8. **Kinematic control validation.** Left: sampled quadruped robot and robotic arm from the dataset. Right: two interpolated novel robot shapes under action control. For visualization, we sweep the first six joints one by one.